Pressure response and phase transitions during a release of high pressure CO_2 from an industrial-scale pipeline

Xiaolu Guo [a], Jianliang Yu [a]*, Xingqing Yan [a], Yongchun Zhang [b], Shaoyun Chen [b], Haroun Mahgerefteh [c], Sergey Martynov [c], Alexander Collard [c], Christophe Proust [d]

a. School of Chemical Machinery, Dalian University of Technology, Dalian, 116024,China

b. School of Chemical Engineering, Dalian University of Technology, Dalian, 116024, China

c. Department of Chemical Engineering, University College London, London WC1E 7JE, UK

d. INERIS, Parc Technologique ALATA, Verneuil-en-Halatte BP 2, 60550, France

Abstract: As part of the Carbon Capture and Storage (CCS) process, pipeline transportation of dense phase CO2 is the safest and most economic option for delivering captured CO2 to a storage site .However, in the event of pipeline rupture an enormous mass of CO2 may be released very rapidly, presenting several risks to the pipeline and surrounding population including the significantly increased risk of brittle fracture in the pipe wall. The study of pressure variation and phase change in CO_2 during pipeline blowdown can contribute to the understanding of brittle fracture initiation and propagation, as well as downstream CO_2 diffusion behaviour. As part of the CO2QUEST project, a reusable, industrial scale pipeline experimental apparatus with a total length of 258 m and the inner diameter of 233 mm was fabricated to study CO_2 pipeline blowdown. A dual-disc blasting device was used to remotely control the opening of the pipeline, three different orifice diameters were used in experiments (15 mm, 50 mm and Full Bore Rupture). Different initial conditions in the inventory were achieved by heating the charged

* Corresponding author.

Tel: +86 411 84986281; *E-mail address*: yujianliang@dlut.edu.cn (J. Yu)

pipeline and by varying the mass of CO_2 used. The instantaneous pressure response following release was measured with high frequency pressure transducers the overall depressurization process was recorded with low frequency transducers. Variation in fluid temperature was also recorded. Six groups of CO_2 pipeline release experiments were conducted with initially gaseous and dense inventories, the variation in fluid pressure and temperature was recorded and phase transitions observed and analysed for each release.

Keywords: CO_2 release, Pressure response, Phase transition, large scale pipeline blowdown.

1. Introduction

Following the Copenhagen Climate Change Conference (2009) there is a broad political consensus to limit the rise in global temperatures to 2 °C above pre-industrial levels. This requires a 50-80 % reduction in CO_2 emissions by 2050 [1]. Carbon Capture and Storage (CCS) is a process by which waste CO2 is captured from large emitters and stored underground, thus reducing direct emissions to the atmosphere [2] and mitigating the environmental impact of fossil fuels.

As a part of the CCS chain, pipeline transportation of CO2 from emitter to storage site is considered the safest and most efficient transportation option [3]. The large scale implementation of CCS will require large transportation networks, potentially between 95,000 and 550,000 km of CO_2 pipelines by 2050 [4]. Safety issues surrounding the operation of CO_2 pipelines are expected to be complex compared to current practice [5,6]. Additionally, CO_2 transmission pipelines may be expected to suffer from accidental releases caused by defects such as mechanical damage, corrosion, construction or material defects, soil movement or even operational mistakes in a similar fashion to hydrocarbon pipelines, for example[6].

Understanding the processes occurring inside a CO_2 pipeline during outflow is essential to investigating fracture propagation and atmospheric dispersion of the inventory [12-16]. For an initially high pressure inventory, whether gaseous, dense phase or supercritical, there is likely to be a complex phase-transition as CO_2 decompresses during pipeline blowdown [10]. The rupture of a CO2 pipeline will result in a series of expansion waves that propagate into the undisturbed fluid in the pipe. Significant Joule-Thomson cooling associated with the rapid expansion of the inventory can result in very low and potentially harmful temperatures in the fluid and pipe wall [11]. The precise tracking of these expansion waves and temperature variations, and their propagation as a function of time and distance along the pipeline, is necessary to predict a pipeline's propensity to fracture [9]. A pipeline failure (most commonly a puncture) may escalate to a fracture if the force acting on the defect overcomes the fracture toughness of the wall material. The fracture may be either in the ductile or brittle regime depending on the nature of the rupture [8].

In order to develop accurate models for predicting the depressurization and phase transition behavior during CO_2 pipeline blowdown, several experimental research programs have been performed. A large scale underground pipeline rupture test was carried out in the COSHER joint industry project to study pipeline depressurization and dispersion of initially dense phase CO_2, with a 219.1 mm diameter pipeline loop was fed from both ends by a 148 m^3 reservoir of CO_2. A fast pressure drop during CO_2 release was observed after the inventory reached saturation conditions [17]. On behalf of Natioinal Grid at the Spadeadam Test Site, three West Jefferson Tests were conducted to investigate ductile fracture propagation in pipelines transporting liquid or dense phase CO_2. The two factors that affect the appearance of a rupture are the length of the initial defect and the ratio of the toughness of the line pipe to the toughness required to arrest a running ductile fracture. [18]. Koeijera et al [19] built a horizontal pipeline with a length of 139 m and an inner diameter of 10 mm in order to study the depressurization behavior of liquid CO_2. Along the pipe, pressure and temperature transducers were installed at 0, 50, 100, 139 m from the closed end. The results show that the pressure drops rapidly at first and then levels off. The rarefaction wave travels across the length of the tube, and which is reflected at the closed end. The wave amplitude diminishes mainly due to wall friction. A depressurization model was developed and its results were compared with experimental data. It is concluded that the model is experimentally verified but more work is needed for further improvement and extending the validity range. [19,20]. Cosham et al [21] performed a program of shock tube tests with CO_2 and CO_2-rich mixtures in order to study decompression behaviour in the gaseous and dense phases. The researchers found that the decompression behaviour of dense CO_2 and CO_2-rich mixtures was very different to that of natural gas, gaseous CO_2 and gaseous CO_2-rich mixtures. The plateau in the decompression curve of dense CO_2 is long [21]. Xie et al developed a circulation pipeline system to study the leakage behavior of high pressure CO_2 flow, which was about 23 m long with an inner diameter of 30 mm. The experimental results indicated that the depressurization process of supercritical-phase is different from that of the gas-phase. The pressure decrease or mass loss of CO_2 in the pipeline was much larger for supercritical leakage due to the higher density. [24]. Huh et al [25] studied the severe pressure and temperature drops during the depressurization of dense CO2 in a 51.96 m long test tube with an inner diameter of 3.86 mm. The results of numerical simulations generated with OLGA were compared against experimental data. It was found that the initial pressure drop was well estimated by OLGA for both pure CO_2 and mixtures, but the numerical simulation did not provide reliable temperature drop predictions [25]. Clausen et al [26] described the results of depressurizing during CO_2 venting with an onshore 50 km long, 24 inch diameter buried pipeline from initially supercritical conditions. Pressure and temperature were measured at the two ends of the pipeline. The depressurization of this pipeline was also simulated with OLGA. According to both experimental data and simulations, the depressurization stayed well above the triple point of CO2, and there was no indication of dry ice formation upstream the two release points. Simulation results deviated from the experimental data after the inventory reached saturation conditions [26]. DNV-GL carried out CO_2 depressurization experiments using a 30 m long, 2 inch diameter stainless steel tube, to study fast depressurization of high pressure liquid CO_2 inventories. This work investigated the minimum temperatures reached during blowdown [27].

This paper presents the results of pipeline blowdown experiments using a 258 m long, 233 mm inner diameter pipeline containing CO2 at various initial conditions. Fluid pressures and temperatures in the pipeline were recorded. The experiments' main objective was to improve the understanding of decompression behavior and phase transition during the release of CO_2.

2. Experiments

2.1 Experimental system

The main components of the experimental setup are shown in Fig.1. The apparatus consists of a single pipeline with a length of 257 m and inner and outer diameters of 233 and 273 mm respectively, a dual-disc blasting pipe with a length of 1 m, a CO_2 injection line, a heating system and two data measurement systems. The main pipe was made of 16MnR steel, which has a minimum allowable temperature of -40 °C, whereas the dual-disc blasting pipe was made of grade 304 stainless steel and its minimum allowable temperature was -196 °C. The pipeline apparatus was designed to operate at a maximum pressure of 16 MPa. 24 concrete column foundations were built to support the pipeline at a height of 1.3 m above ground.

The inventory temperature could be maintained or increased during charging or before experiments using a heating system made up of heating tape and a 50 mm thick thermal insulation layer mounted on the outer pipe surface, the tape was controlled via six temperature controllers. The heating tape power was 50 kW. The heating system was designed to vary the initial temperature of the inventory from 0 to 40 °C.

To open the pipeline and initiate experiments a dual disc blasting device is used. This device is 1 m long and consists of two rupture discs and two disc holders, a solenoid valve and two pipe sections (Section 1 with a length of 0.6 m; Section 2 with a length of 0.3 m) connected by a flange and bolts. A schematic of the dual-disc blasting device is shown in Fig. 2. The pipeline was charged with the appropriate mass of inventory for each experiment and the heating coils used to achieve the desired initial conditions. The pressure P2 in section I was maintained proportionally to the pressure P1 inside the main pipeline. To initiate the experiment, the pressure P2 in section I was rapidly raised, forcing the disc B to break, resulting in the near simultaneous rupture of disc A. Because the length of the dual-disc device (1 m) is much shorter than the main pipeline (257 m), its influence on pressure and temperature measurements in the main pipe can be ignored.

The recoil-shock created when initiating full bore rupture (FBR) experiments was significant. A reinforced anchor device was designed and installed to hold the release end of the pipeline firmly in place, as shown in Fig. 3. The device consisted of steel frames, steel plate, and anchor bolts anchored firmly to the concrete foundation. The reacting force and frictional force of the reinforcement device could resist an acting force of more than 400 kN.

2.2 Pipeline Instrumentation

Various instruments were installed along the pipeline, including 4 low frequency pressure sensors, 8 high frequency pressure sensors, 18 thermocouples on the upper half of pipeline, 6 thermocouples on the bottom half of pipeline and 12 thermocouples on the outer wall of pipeline. Pressure change in the overall process was measured using PPM-S322G pressure transducers with a frequency response of 1 kHz and an accuracy of 0.25 %FS of full scale. Pressure change at the beginning of release was measured using PPM-S116B-0EM pressure transducers with a frequency response of 100 kHz and an accuracy of 0.25 %FS of full scale. Temperature was measured using K-type thermocouples which had a response time of 100 ms and a range of -200 °C to 1300 °C, and uncertainty of $\pm$1 °C. The installing angle of measurement points are shown in Fig. 4.

Data was recorded using two independent measuring systems, an NI cRIO-9025 system which was used to simultaneously sample 4 low frequency pressure sensors and all the thermocouples and an NI cDAQ-9188 system which was used to sample 8 high frequency pressure sensors. The NI cRIO-9025 system consisted of one 9025, four 9144 chasses and twelve 9219 modules for temperature and pressure signal acquisition. The 5 chasses were connected using ordinary internet access cable. The communication protocol used EtherCAT at 110 ms/sample to ensure synchronised data gathering. All of the data acquired would be cached in the host 9025. The NI cDAQ-9188 system consisted of two 9188 of 4 channels with a high-speed of 500 kS/s. LabVIEW software was used to transfer the data from the 9025 or 9188 to a local computer by Ethernet.

2.3 Experiments Conducted

In this paper, three groups of CO_2 release experiments were performed to investigate decompression behaviour and phase transition during the release of CO_2 from a pipeline. Each group used initially vapour and dense phase CO2. Three different orifice diameters were also used for each group of tests; 15 mm, 50 mm and Full Bore Rupture (FBR). Thus six experiments in total were conducted. The initial experimental conditions of the six tests are presented in Table 1. Table 2 reports the instruments from which data is available for the listed experiments, including instrument type, number and location.

3. Experimental results and discussions

In this section the results of six release experiments with three different orifice sizes (15 mm, 50 mm and FBR) are described and the recorded pressure response and phase transition data analysed. In all the following figures a rightward pointing arrow ("→") indicates decompression wave propagation from the discharge end to the closed end of the pipe, while a leftward pointing arrow ("←") indicates decompression wave propagation from the closed end to the discharge end. The numbers above the arrows represent the times for the decompression wave to travel the length of the pipe and their propagation velocities in the 1st and 2nd periods. Three kinds of pressure response parameters are defined as follows: (1) The pressure drop amplitude (ΔPd) is the difference between the maximum pressure front the depressurization wave and the minimum pressure behind the depressurization wave. (2) The pressure rebound amplitude (ΔPr) is the difference between the minimum pressure behind the depressurization wave and the recovery pressure following depressurization. (3) The quasi-static pressure (Pqs) is the recovery pressure following depressurization.

3.1 Gas phase tests

3.1.1 Pressure response

Fig. 5 shows the evolution of fluid pressure after rupture for tests 1, 2 and 3. The total depressurisation times for each experiment are 1946 s, 159 s and 15 s respectively. It may be observed for tests 1 and 2 that the pressure gradient along the length of the pipe is small during decompression, this is not the case for test 3.

In the magnified regions of Fig. 5(a) and (b), the pressure response processes recorded by P2, P5, P7 and P9 at the beginning of tests 1 and 2 are presented. In the 1st period of tests 1 and 2 the decompression wave propagates from the orifice to the closed end at the local speed of sound in the inventory. Behind the decompression wave the inventory pressure drops rapidly. Following the pressure undershoot droplet formation and gasification causes the pressure to recover almost to the initial Pqs in both tests. ΔPf and ΔPr reduce greatly with the increase in distance from the measured point to the orifice. In the 2nd period of tests 1 and 2 the reflected decompression wave travels from the closed end of the pipe towards the rupture end, causing a further decrease in pressure from P9 to P2 in turn. The inventory achieves a second Pqs. ΔPf and ΔPr are fractionally greater with increasing distance from the orifice and the value of Pqs nearer the orifice was affected by the decompression wave and was below the overall Pqs. On the whole, with the decompression wave reflecting repeatedly, ΔPf, ΔPr and Pqs reduced gradually until the pressure drop and rebound inside the pipeline were no longer obvious. Comparing the pressure response parameters of tests 1 and 2, ΔPf of the two were very close, but ΔPr of test 2 (50 mm orifice) was smaller than that of test 1 (15 mm orifice). Pqs of tests 1 and 2 reduced about 0.01 MPa and 0.11 MPa respectively following each passage of the decompression wave.

Fig. 5 (c) shows the variation of fluid pressure with time for test 3. After rupture, the decompression wave propagates with an initial speed of 242.43 m/s. The intersection of curve 1 with the pressure histories indicates the times at which droplets form at each location in the gaseous inventory. ΔPf from P2 to P9 decreased from 1.79 MPa to 0.62 MPa successively. After droplets formed the rate of pressure loss in the pipe decreased to about 2.47 MPa/s. The passage of the reflected decompression wave past each transducer, indicated by the intersection of the pressure histories with curve 2, caused an increase in the rate of recorded pressure drop.

Fig. 6 shows the pressure change rate curve in 1st period of tests 1, 2 and 3. For tests 1 and 2, after undershoot the pressure change rates at P2, P5, P7 and P9 sharp increased to the maximum value and soon back to zero. This phenomenon is caused by droplet gasification. The minimum and maximum value of the pressure change rate decreased successively with increasing distance from the orifice. For P2, P5, P7 and P9, the amplitude of the pressure rise rate was much larger than that of the pressure drop rate, and the duration time of the pressure rise was more shorter than that of the pressure drop. Comparing the pressure change rates of tests 1 and 2, the minimum value of test1 was smaller than that of test2, but the maximum value of test1 was much greater than that of test2. For test3, due to no pressure rebound, the pressure change rate at P2, P5, P7 and P9 only had a drop. For P2, P5, P7 and P9, the amplitude of the pressure drop rate decreased successively and the duration time of the pressure drop became shorter with increasing distance from the orifice.

3.1.2 Phase transition

Fig. 7 plots the evolution of fluid properties on the pressure-temperature phase diagram for tests 1, 2 and 3. Upon rupture, the instantaneous pressure drop was accompanied by the formation of droplets, which caused the sharp temperature fall. The high environment temperature made the droplets vaporise rapidly and caused the pressure rebound or stagnation. Due to the rapidity of this process it was not captured by the temperature thermocouples as their response time was too great. In test1, the overall temperature drop amplitude was not obvious due to the small orifice diameter. In test2, the lowest temperatures recorded by Tf18 and Tf18d were -16 °C and -26 °C respectively. The lowest temperatures at the top and bottom of the pipe at locations 7.4 m, 54.2 m and 62.1 m from the orifice were similar and fell to 23 °C, 22 °C and 21 °C respectively. as indicated by the recorded thermodynamic trajectories of tests 1 and 2, no phase change was observed. In test 3, the lowest values of Tf2, Tf2d, Tf4 and Tf4d dropped to 3 °C, 0 °C, 5 °C and 2 °C when the pipeline pressure dropped to 1.56 MPa, and the lowest values of Tf16, Tf16d, Tf18 and Tf18d fell to - 56 °C, -42 °C, -64 °C and -69 °C when the pipeline pressure dropped to 0.23 MPa, which suggested that the gaseous CO_2 at the pipeline end transformed to the gas-liquid phase in the last period of test 3.

3.2 Dense phase test

3.2.1 Pressure response

Fig. 8 shows the pressure evolutions for tests 4, 5 and 6. The total depressurisation times of each experiment were 7300 s, 482 s and 40 s respectively. As shown in Fig. 10(a) and (b), the decompression process for tests 4 and 5 are very similar. For test 4 and test 5, during phase I of decompression a sharp decline in pressure is observed for both tests, lasting about 34 s and 4.7 s respectively. During phase II of decompression, the inventories achieve saturation pressure (P_S), initially at pressures of 5.08 MPa for test 4 and 5.02 MPa for test 5. Fluid pressures and temperatures then decline along the saturation line for duration times of circa 5838 s and 363 s respectively. When inventory properties reach the triple point the 3rd phase of decompression begins, this 3rd phase lasts about 1428 s and 119 s respectively for tests 4 and 5.

As shown in the magnified regions of Fig. 8(a) and (b), the pressure drop processes of decompression in phase I consisted of about 40 and 4 passes of the decompression wave for tests 4 and 5 respectively. With the propagation of decompression wave, the pressure fluctuation gradually weakened until it disappeared at the end of phase I. During the pressure response process of the 1st period of the dense tests there was an obvious slowdown between sharp decline and rapid rise compared to that seen in tests 1 to 3. Comparing the pressure response parameters of the 1st period of tests 4 and 5, ΔPf of the two were similar, but ΔPr of the former was higher than that of the later, and the Pqs of 9.04 MPa for test 4 was higher than the Pqs of 7.67 MPa for test 5.

As shown in Fig. 8(c), during phase I of decompression, the pressure inside the pipeline sharply dropped to the saturation pressure, the rate of pressure loss then slowed down. During phase II of decompression a significant pressure gradient was recorded along the length of the pipe. In phase III of decompression, the rate of pressure drop increased due to the formation of dry ice, especially was instinct near the pipe closed end.

Fig. 9 shows the pressure change rate curve in 1st period of tests 4, 5 and 6. For tests 4 and 5, the minimum value of the pressure change rate decreased successively with increasing distance from the orifice. The maximum value of the pressure change rate at P2 was much smaller than that at P5, P7 and P9. For P5, P7 and P9, the amplitude of the pressure rise rate was much larger than that of the pressure drop rate, but it's opposite at P2. The wide fluctuations of the pressure change rate was caused by bubble nucleation. For teat6, it's pressure change rate curve in 1st phase was similar to that for test3. However, the amplitude of the pressure drop rate along the pipe of test6 was much greater than that of test3, while the duration time of the pressure drop of test6 was shorter than that of test3. This suggested that the bubble nucleation rate was much greater than the droplet gasification.

3.2.2 Phase transition

Fig. 10 shows the evolution of fluid pressure and temperature plotted on the CO2 phase diagram for tests 4 to 6. Point A indicates the initial phase of each experiment, and the points B and C are the locations of phase changes. After the start of release, due to the low compressibility of dense CO_2 the pressure inside the pipeline fell rapidly to the saturation pressure i.e. from point A to B, corresponded to phase I of decompression. The fluid temperature drop was not large as the dense (liquid) CO_2 couldn't release its heat fast enough. During phase II of decompression the saturation properties evolve from points B to C. Due to the large release rate the measured temperature inside the pipeline tended to shift away from the saturation temperature, indicating the fluid was superheated. . At point C, the inventory reached the CO_2 triple point pressure (0.52 MPa), the subsequent generation of the dry ice at the bottom of the pipeline made the flow phase change to gas-solid flow. For test 4, Tf2, Tf4, Tf16 and Tf18 started to deviate from the saturation line at the point B and Tf2d, Tf4d, Tf16d and Tf18d started to deviate from the saturation line at the point C .This result showed that the transition from gas-liquid phase CO2 to gas CO2 during phase II at the top of the pipe appeared in advance of that at the bottom of the pipe. The phase transition along the length direction of the pipeline wasn't much different during the small bore release. For test 5, Tf2, Tf4, Tf9, Tf18, Tf2d, Tf4d, Tf9d and Tf18d started to deviate from the saturation line when the pressure reached 4.96 MPa, 4.93 MPa, 4.90 MPa, 0.52 MPa, 1.42 MPa, 1.36 MPa, 1.01 MPa, 0.52 MPa. This result showed that The gas-liquid phase CO_2 near the orifice deviated from the saturation line and turn into gas at first, subsequently happened far from the orifice with the pressure decline continuously. Meanwhile, this transition appeared at the top of the pipe before that at the bottom of the pipe. For test 6, Tf2, Tf2d, Tf4 and Tf4d started to deviate from the saturation line when the pressure reached 0.69 MPa and Tf16, Tf16d, Tf18 and Tf18d started to deviate from the saturation line when the pressure reached 0.10 MPa. This result showed that the phase transition at the top and bottom of the pipe was similar during the full bore release due to the large release rate. . The lowest temperatures of test4, test5 and test6 were -53 °C, -66 °C and -72 °C respectively. This result indicate that the lower the minimum temperature reached in the overall release process with the bigger orifice diameter.

4. Conclusions

This article has presented the results of an experimental study of pressure response and phase transition during CO_2 pipeline blowdown. Experiments were conducted using CO2 in initially gaseous, dense and supercritical phases with three different orifice sizes (15 mm, 50 mm and FBR) for a total of six experiments. From this experimental study, selected conclusions are presented as follows:

(1) In all experiments the rapid expansion of the high pressure CO_2 at the orifice resulted in a decompression wave which propagated from the orifice to the closed pipeline end, where it subsequently reflected. Passage of the decompression wave through the inventory caused the pressure undershoot, rebound or slowdown successively, and reached the quasi static pressure level. Moreover, the nearer to the orifice, the longer the quasi static pressure level was maintained.

(2) In the gaseous CO_2 releases, the pressure fall, rebound or slowdown was accompanied by droplet formation and rapid gasification. During the depressurization process, the CO_2 phase was generally gaseous near the orifice. When the release diameter was increased, the P-T curve would be close to the saturation line and the gas-liquid CO_2 would appear near the pipe end and the lowest temperature of the CO_2 at the bottom of the pipe was lower than that at the top.

(3) In the dense CO_2 releases, the pressure undershoot, rebound or slowdown occurred as the dense phase CO_2 transformed into a gas-liquid CO_2 mixture. With larger orifice diameters, a greater proportion of inventory in the pipeline remained in the saturation state and the lowest temperature achieved in the overall release process was lower. When the pressure fell to the CO_2 triple point, the CO_2 phase was mainly gas-solid with dry ice forming at the bottom of the pipeline.

Acknowledgements

The authors would like to acknowledge the funding received from the European Union Seventh Framework Programmes FP7-ENERGY-2009-1 under grant agreement number 241346 and FP7-ENERGY-2012-1STAGE under Grant agreement 309102.

References

[1] IPCC. Climate Change 2007: Mitigation of Climate Change. Contribution of Working Group III to the Fourth [Z] . Assessment Report of the Intergovernmental Panel on Climate Change. 20 07

[2] Haszeldine RS. Carbon Capture and Storage: How Green Can Black Be? Nature 2009; 325:1647-1652.

[3] IPCC. IPCC special report on carbon dioxide and storage. Technical Report; 2005.

[4] IEA. Energy Technology Perspectives 2012: Pathways to a Clean Energy System; 2012.

[5] Koornneef J, Spruijt M, Molag M, Ramirez A, Faaij A. Turkenburg W. Uncertainties in risk assessment of CO_2 pipelines. Energy Procedia 2009; 1:1587–1594.

[6] Duncan IJ, Wang H. Estimating the likelihood of pipeline failure in CO_2 transmission pipelines: New insights on risks of carbon capture and storage[J]. International Journal of Greenhouse Gas Control 2014; 21: 49-60.

[7] Mahgerefteh H, Brown S, Denton G. Modelling the impact of stream impurities on ductile fractures in CO_2 pipelines. Chemical Engineering Science 2012; 74:200-210.

[8] Mahgerefteh H, Zhang P, Brown S. Modelling brittle fracture propagation in gas and dense-phase CO2 transportation pipelines. International Journal of Greenhouse Gas Control 2016; 46: 39-47.

[9] Woolley RM, Fairweather M, Wareing CJ, Proust C, Hebrard J, Jamois D, Narasimhamurthy V D, Storvik IE, Skjold T, Falle SAEG, Brown S, Mahgerefteh H, Martynov S, Gant SE, Tsangaris D M, Economou IG, Boulougouris GC, Diamantonis NI. An integrated, multi-scale modelling approach for the simulation of multiphase dispersion from accidental CO_2 pipeline releases in realistic terrain[J]. International Journal of Greenhouse Gas Control 2014; 27:221-238.

[10] Woolley RM, Fairweather M, Wareing CJ, Falle SAEG, Mahgerefteh H, Martynov S, Brown S, Narasimhamurthy VD, Storvik IE, Sælen L, Skjold T, Economou IG, Tsangaris DM, Boulougouris GC, Diamantonis N, Cusco L, Wardman M, Gant SE, Wilday J, Zhang YC, Chen SY, Proust C, Hebrard J and Jamois D. CO_2PipeHaz: quantitative hazard assessment for next generation CO_2 pipelines. Energy Procedia 2014, 63:2510–2529.

[11] Rian KE, Grimsmo B, Laksa B, Vembe BE, Lilleheie NI, Brox E, Evanger T. Advanced CO_2

dispersion simulation technology for improved CCS safety. Energy Procedia 2014; 63: 2596-2609.

[12] Molag M, Dam C. Modelling of accidental releases from a high pressure CO_2 pipelines. Energy Procedia 2011; 4:2301-2307.

[13] Lund H, Flatten T, Munkejord ST. Depressurization of carbon dioxide in pipelines – models and methods. Energy Procedia 2011; 4:2984-2991.

[14] Aursand E, Aursand P, Berstad T, Dørum C, Hammer M, Munkejord ST, Nordhagen HO. CO_2 pipeline integrity: A coupled fluid-structure model using a reference equation of state for CO_2. Energy Procedia 2013; 37:3113-3122.

[15] Martynov S, Brown S, Mahgerefteh H, Sundara V. Modelling choked flow for CO_2 from the dense phase to below the triple point. International Journal of Greenhouse Gas Control 2013; 19:552-558.

[16] Brown S, Martynov S, Mahgerefteh H, Chen SY, Zhang YC. Modelling the non-equilibrium two-phase flow during depressurisation of CO_2 pipelines. International Journal of Greenhouse Gas Control 2014; 30:9-18.

[17] Ahmad M, Lowesmith B, Koeijer Gd, Nilsen S, Tonda H, Spinelli C, Cooper R, Clausen S, Mendes R, Florisson O. COSHER joint industry project: Large scale pipeline rupture tests to study CO_2 release and dispersion. International Journal of Greenhouse Gas Control 2015; 37: 340–353.

[18] Cosham A, Jones DG, Armstrong K, Allason D, Barnett J. Ruptures in gas pipelines, liquid pipelines and dense phase carbon dioxide pipelines. Proceedings of the 2012 9th International Pipeline Conference; 2012.

[19] Koeijera Gd, Borch JH, Jakobsenb J, Drescher M. Experiments and modeling of two-phase transient flow during CO_2 pipeline depressurization. Energy Procedia 2009; 1:1683-1689.

[20] Drescher M, Varholm K, Munkejord ST, Hammer M, Held R, Koeijer Gd, Barnett J. Experiments and modelling of two-phase transient flow during pipeline depressurization of CO_2 with various N2 compositions. Energy Procedia 2014; 63:2448-2457.

[21] Cosham A, Jones DG, Armstrong K, Allason D, Barnett J. The decompression behaviour of carbon dioxide in the dense phase. Proceedings of the 2012 9th International Pipeline Conference; 2012.

[22] Han SH, Kim J, Chang D. An experimental investigation of liquid CO_2 release through a capillary tube. Energy Procedia 2013; 37:4724-4730.

[23] Han SH, Chang D, Kim J, Chang W. Experimental investigation of the flow characteristics of jettisoning in a CO_2 carrier. Process Safety and Environmental Protection 2014; 92:60-69.

[24] Xie QY, Tu R, Jiang X, Li K, Zhou XJ. The leakage behavior of supercritical CO_2 flow in an experimental pipeline system. Applied Energy 2014; 130:574-580.

[25] Huh C, Cho MI, Hong S, Kang SG. Effect of Impurities on Depressurization of CO_2 Pipeline Transport. Energy Procedia 2014; 63:2583–2588.

[26] Clausen S, Oosterkamp A, Strøm KL. Depressurization of a 50 km long 24 inches CO_2 pipeline. Energy Procedia 2012; 23:256–265.

[27] Vree B, Ahmad M, Buit L, Florisson O. Rapid depressurization of a CO_2 pipeline – an experimental study. International Journal of Greenhouse Gas Control 2015; 41:41–49

Figures

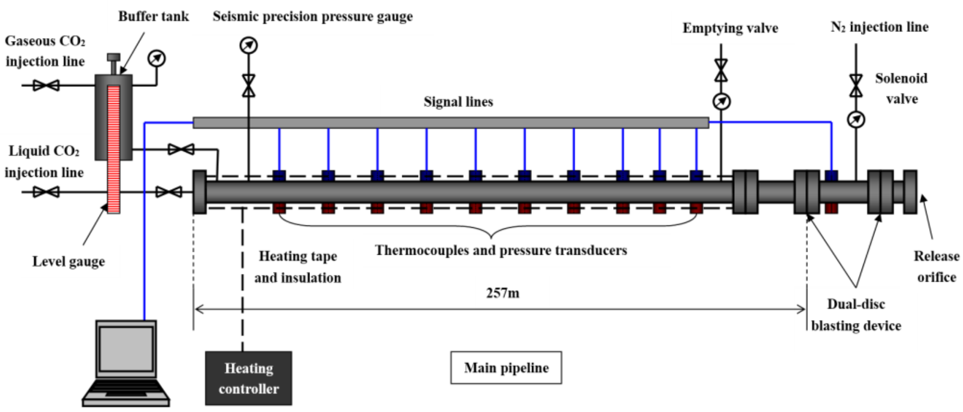

(a) Schematic diagram

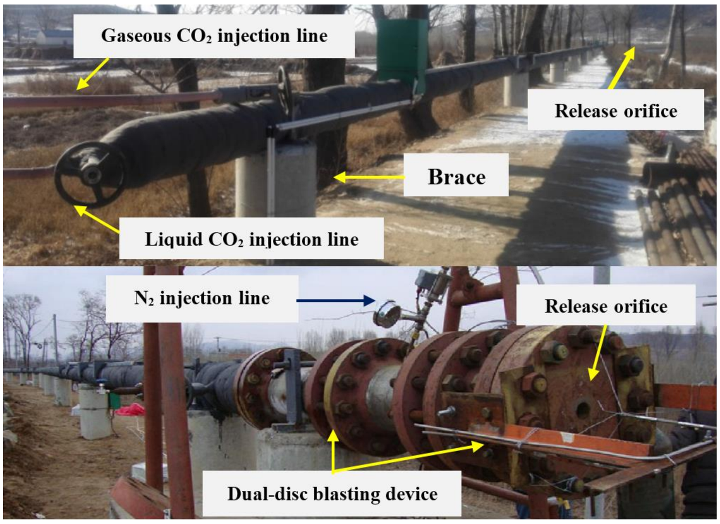

(b) Photograph

Fig. 1 Schematic and scene graph of experimental apparatus

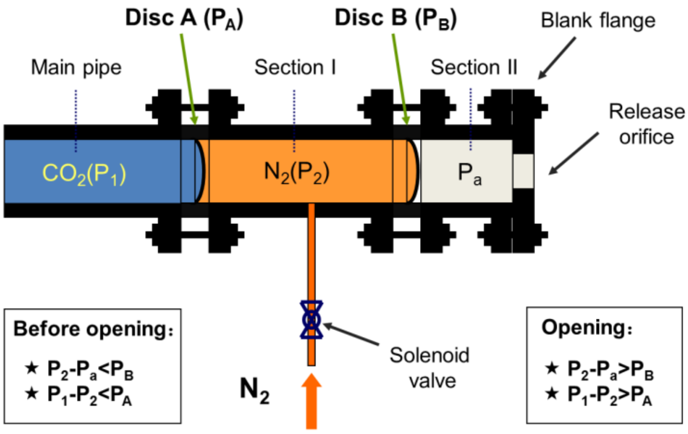

Fig. 2 Schematic of dual-disc blasting device

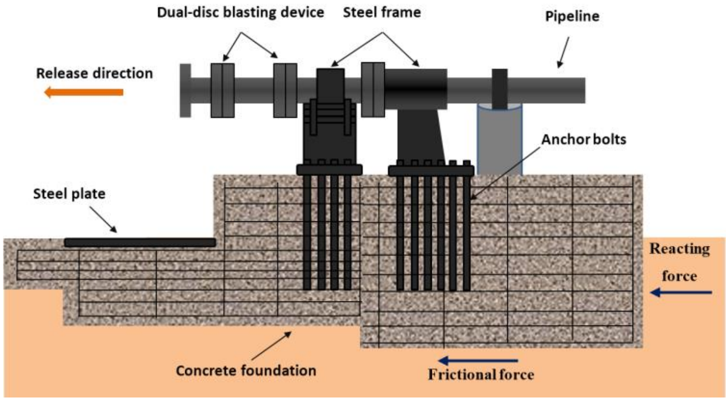

(a) Schematic diagram

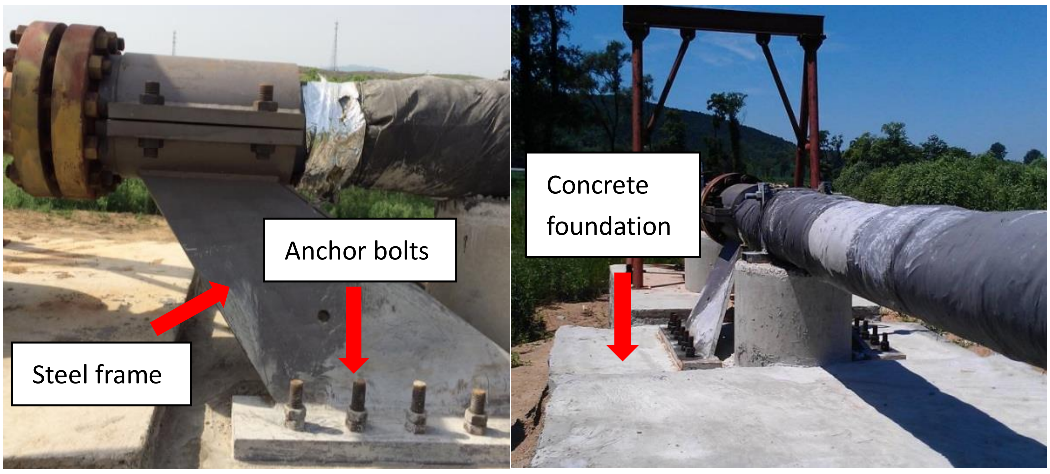

(b) Photograph

Fig. 3 Illustration of the reinforcing device

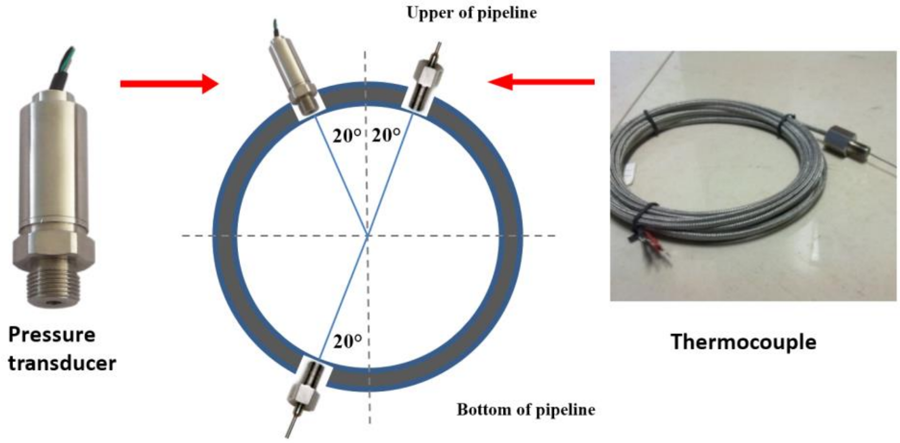

Fig. 4 Measurement point locations

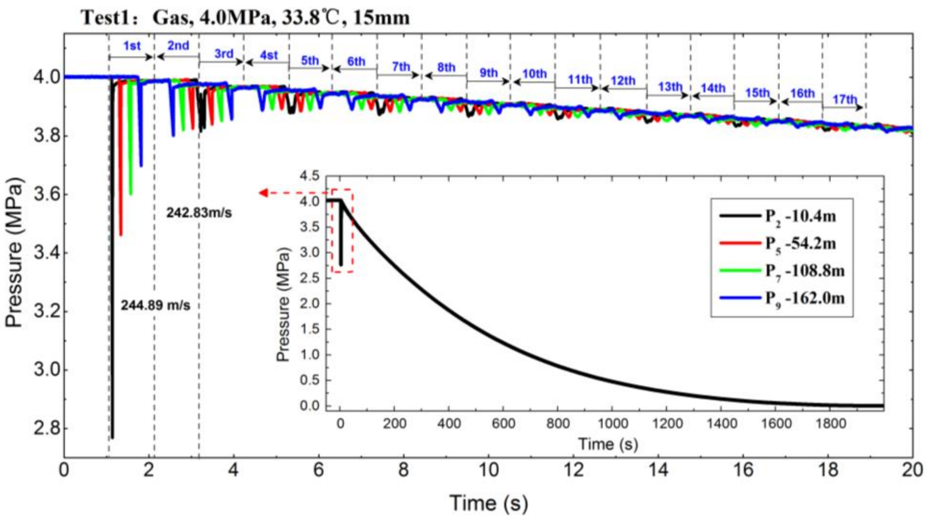

(a) Test1-15 mm orifice

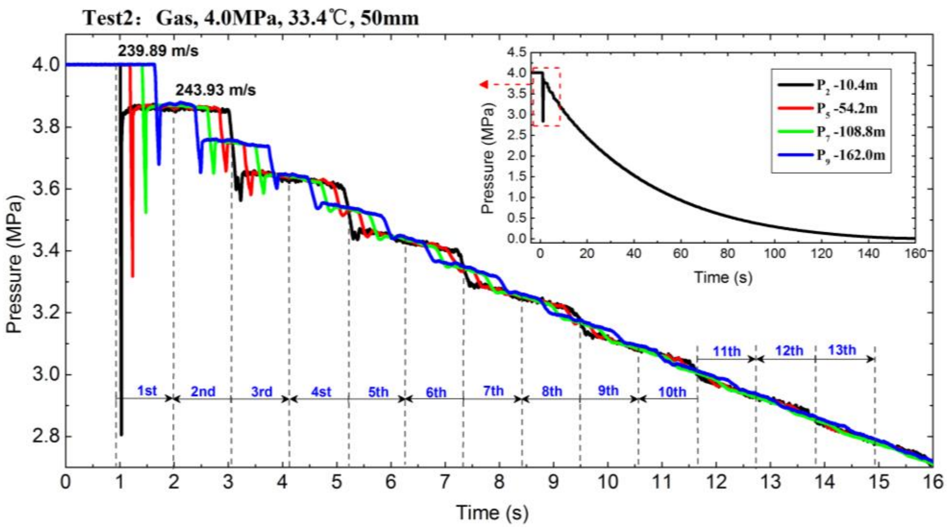

(b) Test2-50 mm orifice

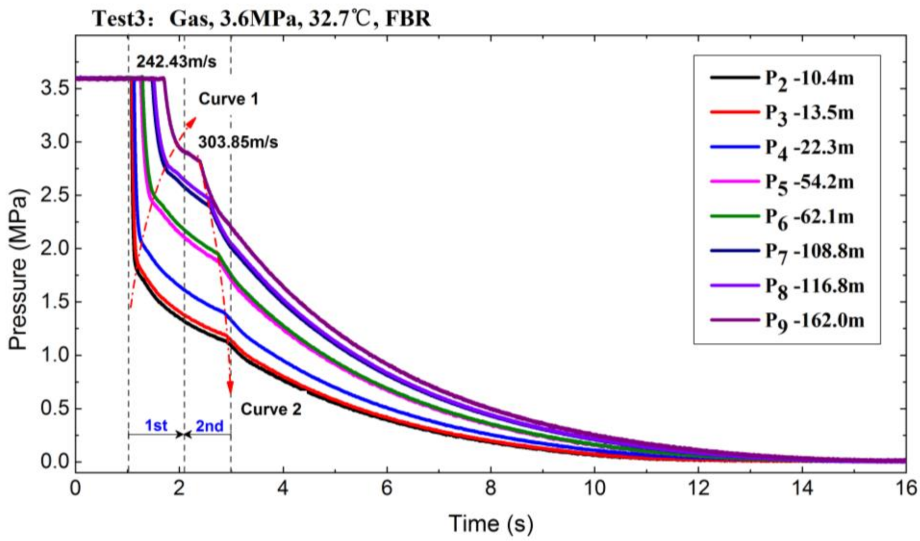

(c) Test3-FBR

Fig. 5 Pressure evolutions of the gas CO_2 release experiments with three different orifices (15 mm, 50 mm and FBR)

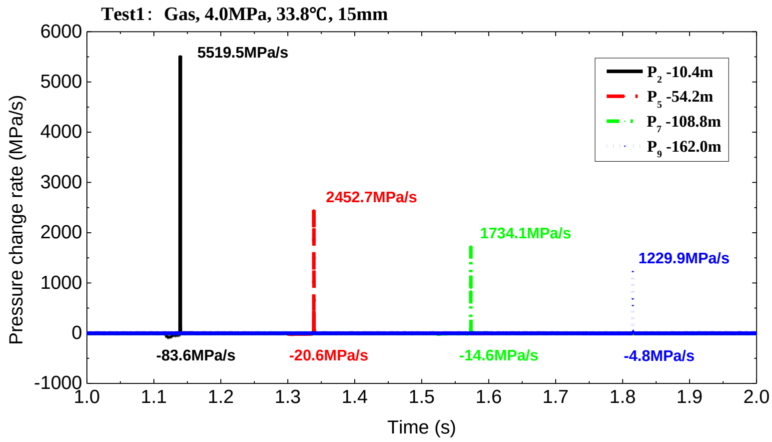

(a) Test1-15 mm orifice

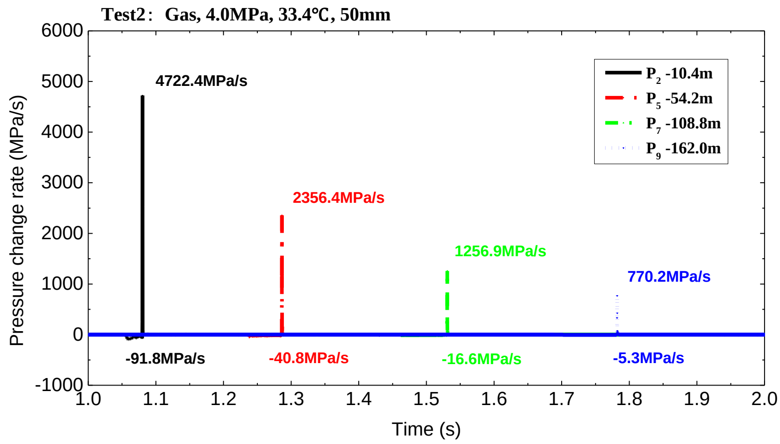

(b) Test2-50 mm orifice

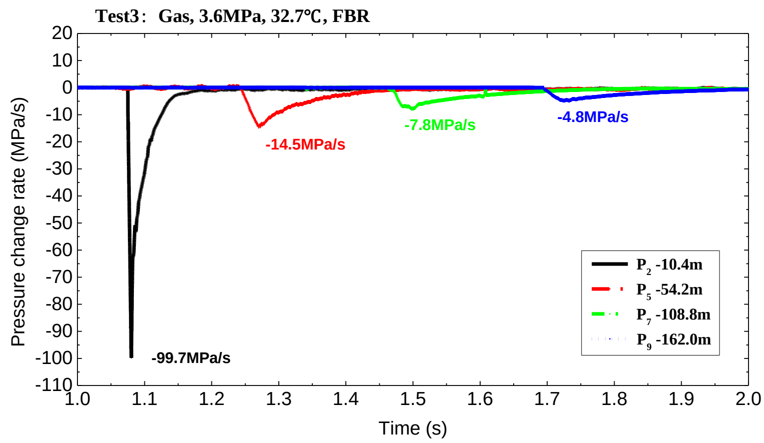

(c) Test3-FBR

Fig. 6 Pressure change rate curve in 1st phase of the gas CO2 release experiments with three different orifices (15 mm, 50 mm and FBR)

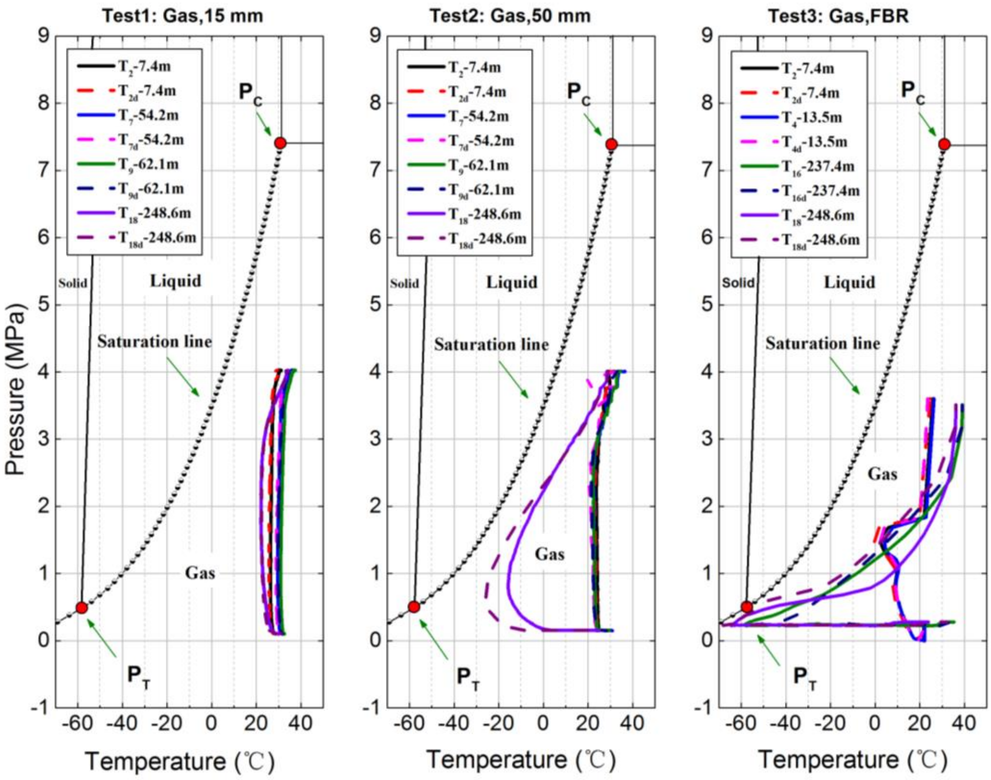

Fig. 7 Pressure-temperature development with three gas CO2 release experiments

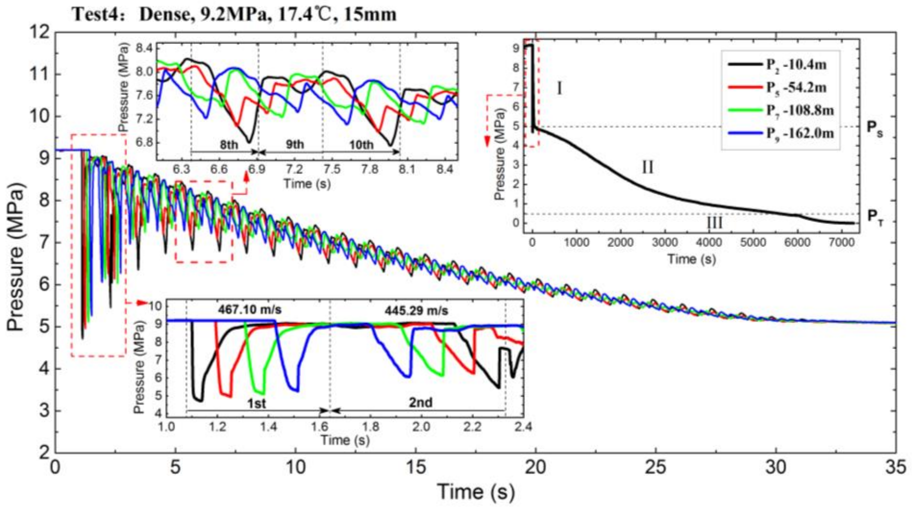

(a) Test4-15 mm orifice

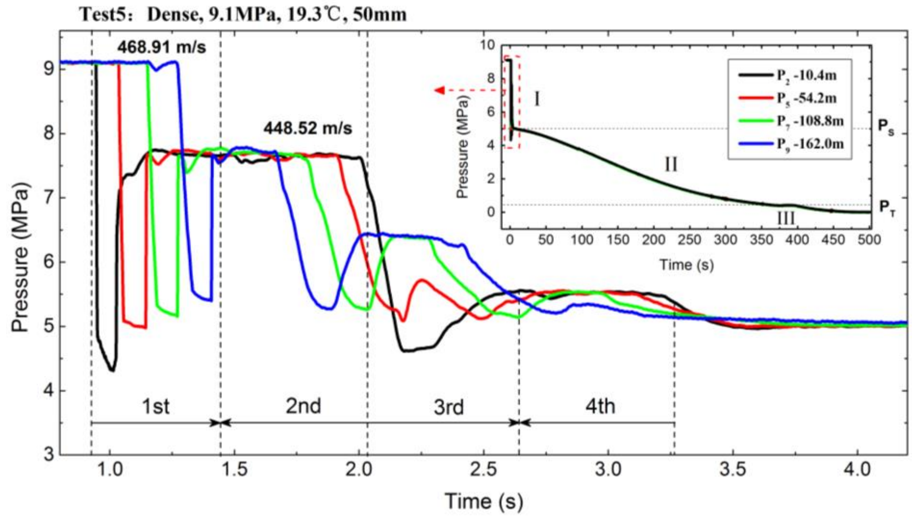

(b) Test5-50 mm orifice

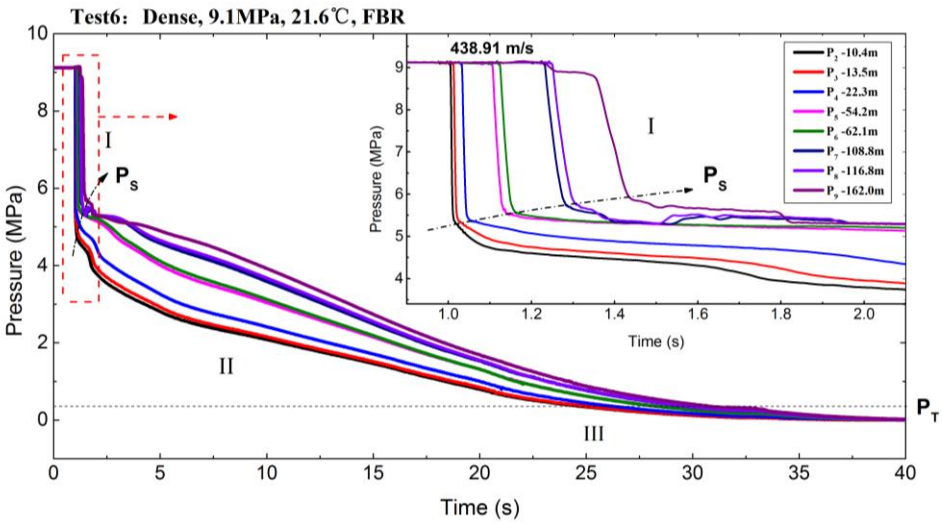

(c) Test6-FBR

Fig. 8 Pressure evolutions of the dense CO_2 release experiments with three different orifices (15 mm, 50 mm and FBR)

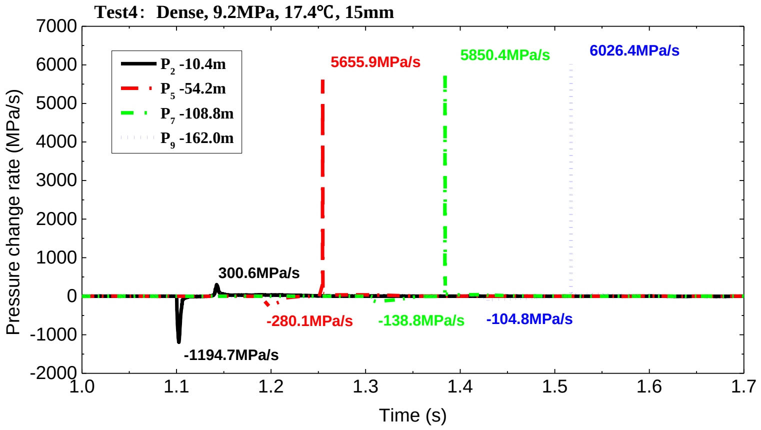

(a) Test1-15 mm orifice

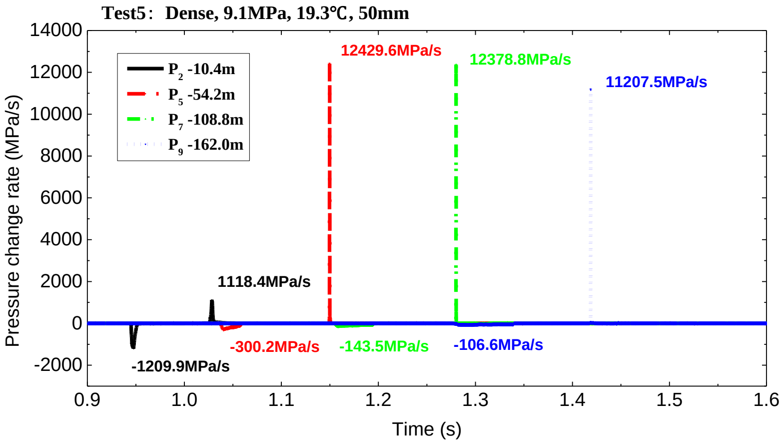

(b) Test2-50 mm orifice

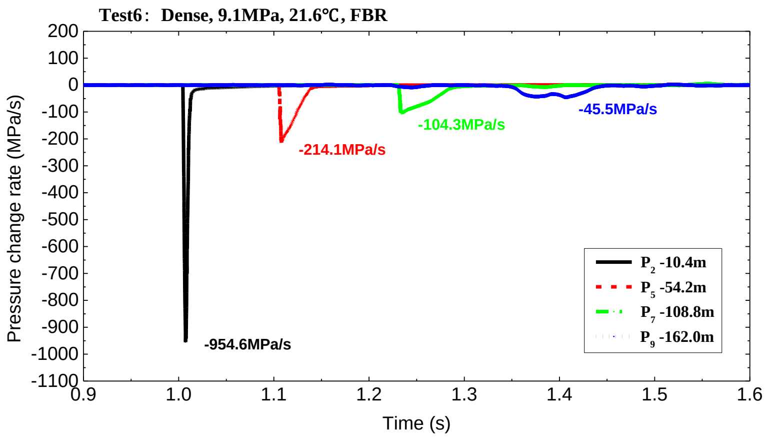

(c) Test6-FBR

Fig. 9 Pressure change rate curve in 1st phase of the dense CO2 release experiments with three different orifices (15 mm, 50 mm and FBR)

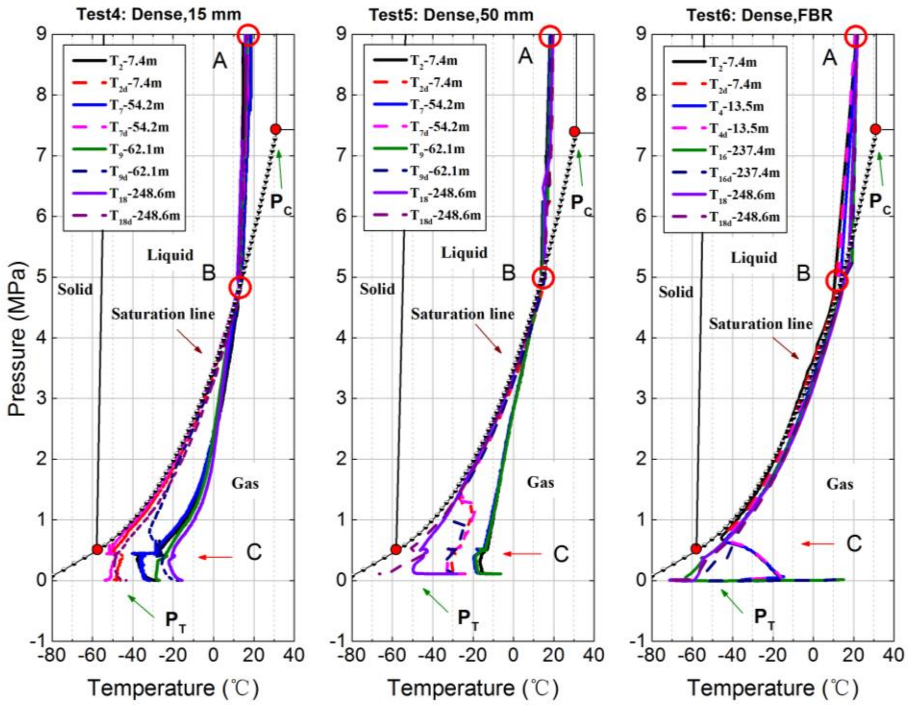

Fig. 10 Pressure-temperature development with three dense CO2 release experiments

Table 1 Experimental conditions

Number	Phase	Pressure (MPa)	Temperature (℃)	Orifice (mm)	Inventory (tons)
Test1	Gas	4.05	33.8	15	0.97
Test2	Gas	4.0	33.4	50	0.96
Test3	Gas	3.6	32.7	FBR	0.84
Test4	Dense	9.2	17.4	15	9.48
Test5	Dense	9.1	19.3	50	9.31
Test6	Dense	9.1	21.6	FBR	9.11